

Spatially Resolving Electron Spin Resonance of π -Radical in Single-molecule Magnet

Ryo Kawaguchi ^a, Katsushi Hashimoto ^{b,c}, Toshiyuki Kakudate ^d, Keiichi Katoh ^e, Masahiro Yamashita ^{f,g}, and Tadahiro Komeda ^{a,c}.

^a Institute of Multidisciplinary Research for Advanced Materials (IMRAM, Tagen), Tohoku University, Sendai 980-0877, Japan

^b Department of Physics, Graduate School of Sciences, Tohoku University, Sendai 980-8578, Japan

^c Center for Science and Innovation in Spintronics (Core Research Cluster), Tohoku University, Sendai 980-8577, Japan

^d Department of Industrial Systems Engineering National Institute of Technology (KOSEN), Hachinohe College, 16-1 Uwanotai, Tamonoki, Hachinohe, 039-1192, Japan

^e Department of Chemistry, Graduate School of Science, Josai University, Sakado, Saitama 350-0295, Japan

^f Department of Chemistry, Graduate School of Science, Tohoku University, Sendai 980-8578, Japan

^g School of Materials Science and Engineering, Nankai University, Tianjin 300350, China

π -Radical Electron Spin, Electron Spin Resonance, Scanning Tunneling Microscope, Single-Molecule Magnet (SMM), TbPc₂

The spintronic properties of magnetic molecules have attracted scientific attention. Special emphasis has been placed on the so-called qubit for quantum information processing. The single-molecule magnet, bis(phthalocyaninato (Pc)) Tb(III) (TbPc₂), is one of the best examined cases in which the delocalized π -radical electron spin of the Pc ligand plays the key role in reading and intermediating the localized Tb spin qubits. Herein, we utilize the electron spin resonance (ESR) technique implemented on a scanning tunneling microscope (STM) and use it to measure local ESR on a single TbPc₂ molecule decoupled from the Cu(100) substrate by 2 monolayers NaCl film to identify the π -radical spin. We detected the ESR signal at the ligand positions at the resonant condition expected for the $S = 1/2$ spin. The result provides direct evidence that the π -radical electron intrinsic to the TbPc₂ molecule is delocalized within the ligands and exhibits intramolecular coupling susceptible to the chemical environment.

The spintronics technique exploiting spin-charge conversion is one of the important techniques used to develop electronic devices based on spin-quantum bits (qubits) to achieve quantum information processing (QIP)^{1,2}. The ideas of quantum spintronics were proposed at early stages^{3,4} and has been extensively used to electrically read-out the quantum information of single spin qubits implemented in the forms of quantum dots⁵, dopants⁶ in semiconductors, and more recently, in a form of a new class of systems referred to as single-molecule magnets (SMMs). The SMM has great potential for the realization of single-molecule qubits because it preserves the magnetization information for a specific time below the blocking temperature⁷. Specifically, one

of the lanthanide (Ln)-based, double-decker Pc SMMs of the TbPc₂ molecule attached in nanogap electrodes successfully demonstrated the quantum manipulation and read-out of the hyperfine coupled electronic ground state $J = \pm 6$ and nuclear spin $I = 3/2$ of the Tb ion through electric transport^{8–10}. The mechanism of this spin-charge conversion was claimed to be based on the key role of the π -radical as the interface between the Tb spin and the conduction electron, manifested by the weak magnetic coupling of the delocalized π -radical electron spin with the localized magnetic moment of Tb 4f⁸ electrons¹¹. These magnetic coupling and delocalization are crucial for designing suitable interfaces for not only spin-charge conversion, but also one-dimensional (1D)^{12–15} or two-dimensional (2D)¹⁶ spin network to achieve QIP; thus, demanding a spatially resolved magnetic characterization of the delocalized π -radical spin within the individual SMM.

Scanning tunneling microscopy (STM) and spectroscopy (STS) revealed the existence of the spin of the TbPc₂ molecule adsorbed on the metal surface based on the observation of the Kondo resonance¹⁷. The Kondo resonance appears owing to the spin screening by the conduction electron that forms the Kondo cloud. However, the information obtained by the Kondo resonance is limited compared with that obtained by a more direct method, such as electron spin resonance (ESR). For example, the Kondo resonance cannot provide direct evidence to attribute its origin to the π -radical spin of $S = 1/2$. Recently, the ESR technique was used in combination with STM (ESR-STM) to identify a magnetic moment in an individual atom at the high-energy resolution (nano-eV range)^{18,19}, which is not easily achieved in STS-based Kondo measurements^{20–22}.

In addition, several STS studies found that the interaction of the π -radical with the substrate alters the intrinsic spin characteristics of the SMM¹⁶. For instance, the ligand spin is quenched when the TbPc₂ molecule is adsorbed on the Co²³ or Ag¹⁵ surfaces. This effect is suppressed by an ultrathin dielectric film of MgO used as an insulating film. This has been demonstrated by ESR-

STM measurements that have resolved the intrinsic spin of atoms^{18,24–26}. However, a recent ESR-STM study showed that the spin character of an SMM, such as iron phthalocyaninato (FePc) molecules, is modified by charge transfer from the metal substrate even when protected by the MgO film^{22,27}. A similar case was also observed in π -radical-based molecules (C₂₂H₁₄) deposited on a MgO/Ag substrate²⁸, thus indicating the imperfect decoupling property of the MgO film. It is required to examine other types of dielectric films to investigate the intrinsic spin characteristics of the π -radical electron at the single molecular level.

In this study, we performed ESR-STM measurements on a single TbPc₂ molecule adsorbed on dielectric 2 monolayer (ML) NaCl films which covered a Cu(100) surface. Even though the MgO film is often employed in ESR-STM studies^{18,24,29,25,26}, we deliberately used 2ML NaCl that has a different and a more versatile nature as an insulating film. The radiofrequency (RF) signal was superimposed on the DC tunneling bias voltage (V_{DC}), and the magnetic field was generated by a superconducting magnet. The STM tip was decorated with a few Fe atoms to be spin-polarized. The ESR spectrum described as the RF-induced tunneling current versus RF frequency showed a sharp ESR signal only upon measurements at the Pc ligand positions within the single TbPc₂ molecule. The peak frequency exhibited a linear dependence on the magnetic field and yielded a *g*-factor equal to 1.84 ± 0.12 . The resonant behavior demonstrates that we spatially and energetically resolved the $S = 1/2$ π -radical electron spin inherent to the Pc ligand of the single TbPc₂ molecule. Furthermore, an intriguing difference appeared from the conventional ESR results, whose mechanism will be discussed in the following section.

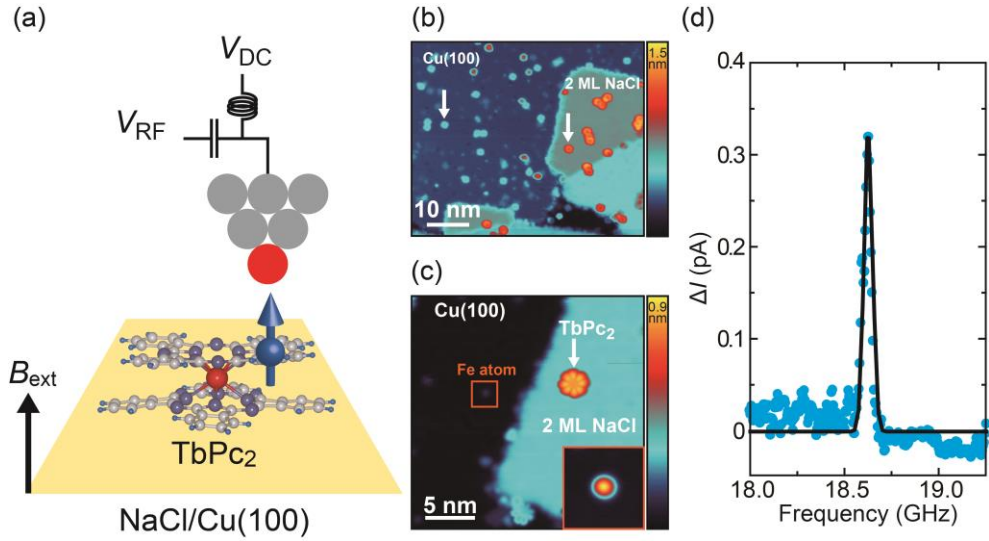


Figure 1. Electron spin resonance-scanning tunneling microscopy (ESR-STM) measurements of single TbPc_2 molecules adsorbed on a $\text{NaCl}/\text{Cu}(100)$ surface. (a) Schematics of the experimental setup. Single TbPc_2 molecule adsorbed on 2 ML $\text{NaCl}/\text{Cu}(100)$ surface is studied using ESR-STM with an out-of-plane external magnetic field (B_{ext}). Radiofrequency (RF) voltage (V_{RF}) is applied to the tunneling junction with a DC bias voltage (V_{DC}) based on the use of a bias Tee. A few Fe atoms (represented by red-filled circles) are picked up by the tip apex from the Cu surface to prepare the spin-polarized magnetic tip. (b) Large-scale constant current STM image of TbPc_2 molecules adsorbed on the 2 ML $\text{NaCl}/\text{Cu}(100)$ and $\text{Cu}(100)$ surfaces. Scanning conditions: $V_{\text{DC}} = -1.5$ V, $I = 24$ pA. The white arrows indicate representative isolated TbPc_2 molecules. (c) Small-scale constant current STM image of a representative isolated single TbPc_2 molecule (marked by a white arrow) adsorbed on the 2 ML $\text{NaCl}/\text{Cu}(100)$ surface. The eight bright lobes correspond to the upper Pc ligand and darker center of the Tb ion. The orange square marks a Fe atom. Scanning conditions: $V_{\text{DC}} = -1.3$ V and $I = 10$ pA. (d) ESR spectrum measured at a lobe position of the TbPc_2 molecule on the 2 ML $\text{NaCl}/\text{Cu}(100)$ surface with an external out-of-plane magnetic field

of 650 mT. ESR-STM conditions: $V_{\text{DC}} = -100$ mV, $I = 10$ pA, $V_{\text{RF}} = 10$ mV. The ESR spectrum is fitted with a Lorentzian function (black curve).

The measurements were conducted with the use of a low-temperature ^3He STM system (Unisoku UHV USM1300) equipped with a superconductor magnet and high-frequency semi-rigid cable which connected the tip bias line (more details of the measurement setup are provided in the Supporting Information (SI), Section 1). Before the ESR-STM measurements, we prepared the spin-polarized STM tip by picking up a few Fe atoms from the Cu surface with the STM tip and then confirmed the spin polarization determined by the asymmetric dI/dV spectrum of the TbPc₂ molecule (see SI Section 2). Figure 1(a) illustrates the experimental setup of ESR-STM to investigate the spin resonance of the single-molecule of TbPc₂. The RF signal voltage (V_{RF}) is superimposed to the DC tunneling bias voltage (V_{DC}) by using the bias Tee, followed by its use in the tunneling junction via the semi-rigid and flexible coaxial cables (see SI Section 1). The frequency-dependent transmission of the RF line, which was determined based on the use of the surface state of the Ag(111) surface³⁰, was compensated by tuning the RF source power (more details of the compensation technique are provided in SI, Section 3) to apply the constant amplitude of the RF voltage (V_{RF}) at the tunneling junction. The tunneling current enhancement at the resonant condition was detected using the lock-in technique in which the RF signal was chopped at a frequency of 431 Hz, and the synchronized tunneling current variation was detected by the lock-in amplifier (see SI Section 3). To decouple the TbPc₂ molecules from a metal substrate electronically, we selected the dielectric NaCl thin film³¹⁻³³. The NaCl film was deposited by thermal evaporation from a Knudsen cell (K-cell) onto the Cu(100) surface at room temperature,

which metal substrate was precleaned following several cycles of Ar⁺ ion sputtering and electron bombardment annealing at 670 K. Subsequently, TbPc₂ molecules were deposited onto the substrate at 50 K from another K-cell. Additionally, Fe atoms were deposited onto the substrate at 30 K by electron-bombardment evaporation to prepare the spin-polarized tip (See SI Section 2). All ESR measurements were completed by minimizing the tunneling current ($I = 10$ pA) and with the application of $V_{DC} = -100$ mV to the tip.

Figure 1(b) shows the STM topographic image of the surface prepared by depositing 2 monolayers (ML) of NaCl film onto the Cu(100) surface followed by the deposition of a submonolayer amount of TbPc₂. On the right side of the STM image, 2 ML NaCl film partially covering Cu(100) was visible, while a bare Cu(100) surface was exposed in other parts. Among the coinage metals, the adsorption energy of TbPc₂ was higher on the Cu surface than on Ag and Au³⁴. Accordingly, an isolated TbPc₂ molecule can be observed easily on the Cu(100) surface (marked by a white arrow, see the left side). The NaCl film provides a smaller adsorption energy when used in conjunction with a TbPc₂ molecule, and the molecule hops on the film and tends to form a dimer or larger cluster. As a result, we can barely see an isolated molecule on the NaCl film as indicated by the white arrow; however, the number of the molecules is equal to 1/3 of that on the Cu surface, as estimated by the statistical analysis over a wider areas (see SI Section 4). In the magnified STM image of Figure 1(c), the TbPc₂ molecule shows a characteristic eight lobe-like shape which appearing on the side of the benzene ring of the Pc ligand. In addition, the Fe atom (indicated by the orange-colored square) deposited to prepare the spin-polarized tip are visible in the optimized color-scale STM topographic image (inset).

We performed ESR-STM measurements on the isolated single TbPc₂ molecule adsorbed on the 2 ML NaCl/Cu(100) surface based on the following measurement conditions: $V_{RF} = 10$ mV, $I =$

10 pA, and $V_{DC} = -100$ mV; these were used in all ESR-STM measurements. Figure 1(d) shows the tunneling current variation (ΔI) obtained on one of the lobes of the TbPc₂ molecule by sweeping the RF frequency from 18.0 GHz to 19.5 GHz under the out-of-plan magnetic field $B_{ext} = 650$ mT, in which a sharp peak around 18.6 GHz exhibits the tunneling current enhancement $\Delta I = 0.3$ pA. By fitting the spectrum with a Lorentzian function (black curve), we determined the linewidth of the peak of 55 MHz and quantified the energy resolution of approximately 100 nano-eV at this ESR-STM condition. The observed peak of the tunneling current appeared only for the TbPc₂ molecule adsorbed on the 2 ML NaCl(100)/Cu(100) surface but not on the Cu(100) surface. This molecule-derived peak was attributed to the ESR driven in the single TbPc₂ molecule according to the following process. The V_{RF} modulated the magnetic-field gradient generated by the spin-polarized tip. At the V_{RF} frequency corresponding to the Zeeman energy lifted by the external magnetic field, the effective oscillating magnetic field imposed by V_{RF} drives the ESR transition between the Zeeman split states. This resulted in changes in the population of the splitting states, and then altered the tunneling magnetoresistance, which can be detected as a tunneling current variation ΔI with the use of a spin-polarized tip¹⁸.

To examine the origin of the resonance peak, we investigated the position-dependent variation of the ESR-STM spectra within the molecule. Figure 2(a) shows the ESR-STM spectra obtained in the two different lobes and at the center of the TbPc₂ molecule, as illustrated by the circles superimposed on the topographic image of the molecule (Figure 2 (b)) with colors that match those of the spectra. The apparent peaks are observed at the same frequency at two different lobe positions, whereas the peak was absent at the center position. This is similar to what we observed previously for the spin-dependent Kondo distribution in the TbPc₂ molecule adsorbed on Au(111), in which the sharp Kondo peak was observed at the lobe position, while it disappeared at the center

position¹⁷. These results suggest that our ESR-STM probed the $S = 1/2$ π -radical electron spin that was distributed on the Pc ligands near the lobe positions, as schematically drawn by the blue ring in Figure 2(c).

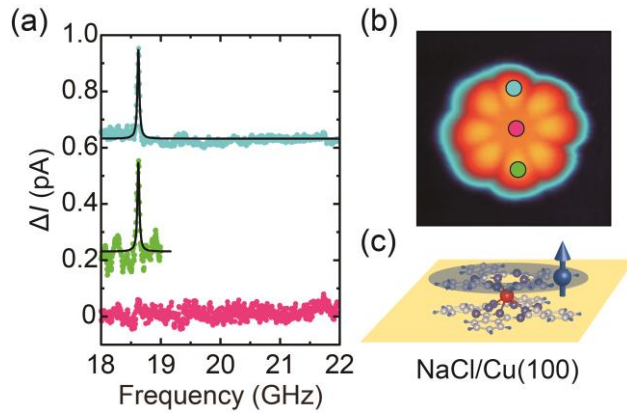


Figure 2. Spatial distribution of ESR signal within a single TbPc_2 molecule. (a) ESR spectra measured at the positions marked with the corresponding color in (b) at $B_{\text{ext}} = 650$ mT. All spectra were acquired at the same conditions: $V_{\text{DC}} = -100$ mV, $I = 10$ pA, and $V_{\text{RF}} = 10$ mV. Each spectrum is shifted vertically for improved visualization. Black curves superimposed on the two spectra are Lorentzian fits. (b) STM image of single TbPc_2 molecule adsorbed on the 2 ML $\text{NaCl}/\text{Cu}(100)$ surface. Scanning conditions: $V_{\text{DC}} = -100$ mV and $I = 10$ pA. (c) Schematics of the π -radical electron spin distribution (blue ring) within the TbPc_2 molecule adsorbed on the 2 ML $\text{NaCl}/\text{Cu}(100)$ surface.

To clarify that the detected peak is the resonance of the π -radical electron spin, we obtained spectra at the same lobe position at different external magnetic fields ($B_{\text{ext}} = 650, 750$, and 800 mT), and showed them in Figure 3(a). As shown, the ESR peak shifts to a higher frequency with an increasing magnetic field. The determined ESR frequencies are plotted as a function of B_{ext} in Figure 3(b), thus indicating the linear Zeeman shift described by $hf = g\mu_{\text{B}}SB_{\text{ext}}$. Herein, h is the Planck's constant, f is the resonant frequency, and μ_{B} is Bohr magneton. The g -factor was obtained from the linear fitting of the plot in Figure 3(b) and is equal to 1.84 ± 0.12 . This is close to the recently reported g -factor value of 2.00 , which was determined by conventional ESR for the ensemble TbPc_2 molecules, such as the single crystal or powder sample, and which identified the electron spin character as π -radical ($S = 1/2$)³⁵. Thus, we conclude that the assignment of our observed ESR features originated from the delocalized π -radical electron spin at the lobe region.

Despite good agreement of g -factor value with the results of the ensemble ESR, we found a significant difference in the zero-field intercept f_0 in Figure 3(b) (inset); our fitting result yielded $f_0 = 1.8 \pm 1.0$ GHz which is one order magnitude lower than the results of the ensemble ESR case ($f_0 = 26.4$ GHz)³⁵. Note that the f_0 differences cannot be attributed to experimental artifacts. In the ESR-STM setup, the stray magnetic field from the spin-polarized tip, so-called the tip field (B_{tip}), can be superimposed on B_{ext} . However, from the tunneling current of 10 pA used in our measurements, B_{tip} can only be equal to a few tens of mT^{24–26}. Additionally, the magnetic hysteresis of the superconductor magnet can yield an error approximately equal to ± 10 mT. These are too small to account for large deviations of zero-field intercept from the ensemble ESR.

For the conventional ensemble ESR measurements, the zero-field intercept is interpreted to be the strength of exchange interaction, which shifts the resonant positions in a parallel manner³⁵. The intramolecular exchange interaction of the TbPc_2 molecule is described as $J_{\text{ex}}\hat{S}^{\text{Pc}} \cdot \hat{J}^{\text{Tb}}$. Herein,

\hat{S}^{Pc} and \hat{J}^{Tb} represent the angular momentum operators associated with the π -radical electron ($S = 1/2$) and Tb ion ($J = 6$), respectively, and J_{ex} is the coupling parameter between them. Therefore, we argue that our observed small intercept of $f_0 = 1.8 \pm 1.0$ GHz is due to the exchange interaction in the isolated single TbPc₂ molecule being significantly weaker than that of the ensemble case.

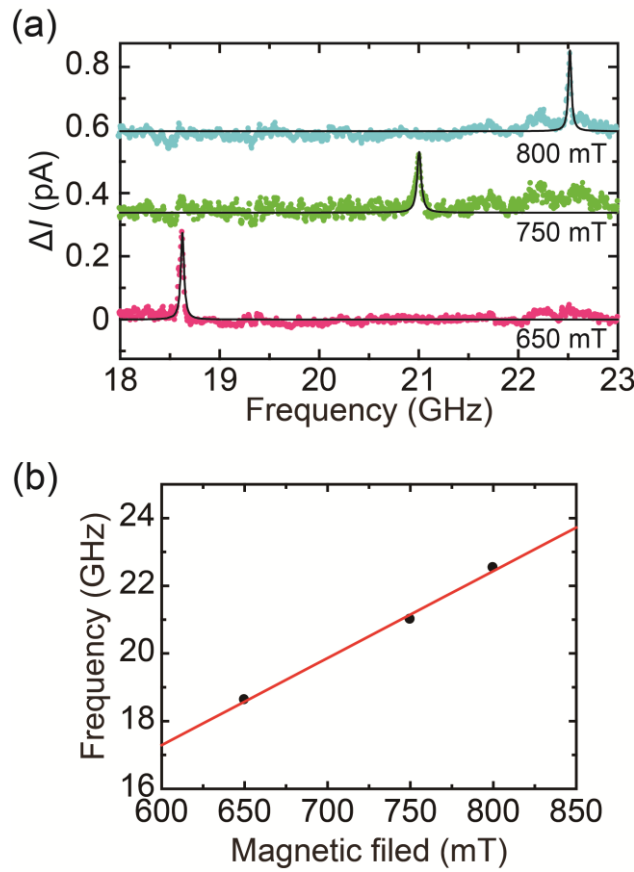


Figure 3. External magnetic-field dependence of the ESR spectra on the ligand of TbPc₂ molecule.

(a) ESR spectra obtained at the same ligand position marked by one of the dots in Figure 2(b) and at the same ESR-STM conditions. Each spectrum is vertically shifted for improved visualization. The solid black curves are obtained from Lorentzian fits. (b) Magnetic field dependence of the resonant frequencies determined in (a).

The possible cause for the weak exchange interaction is the chemical environment of the individual molecule. Specifically, for the single molecule adsorbed on a substrate, the intramolecular electronic orbital is affected by the coupling with the substrate, while being free from the intermolecular interactions relevant to the molecule in the bulk crystal. As a result, the magnetic properties are no longer identical to that in the bulk crystal. In the current experiment, the isolated single molecule was electrically decoupled from the metal substrate by the presence of the insulating film of NaCl that acted as an insulator to suppress the influences attributed to the metal substrate, such as charge transfer or hybridization; thus, the NaCl film preserved the inherent electric properties of the free-standing molecule³¹. Conversely, owing to the dielectric nature of the NaCl film, the long-range polarization effect should deform the electronic structure of the individual TbPc₂ molecule in a manner different from that of the TbPc₂ bulk crystal. A theoretical study showed that upon adsorption on NaCl/Ge, the energy separation of the carbon monoxide molecule HOMO-LUMO gap changes depending on the thickness of the NaCl layer, and is accounted for by the long-range polarization effect originating from the NaCl/Ge interface³⁶. This gap behavior has also been reported in STS experiments on pentacene molecule adsorbed on a NaCl/Cu surface³⁷. Furthermore, the exchange interaction energy within the SMM sensitively changes when the intramolecular charge distribution varies³⁸. Thus, the significant difference in the intramolecular exchange interaction between our and the ensemble ESR result may be

attributed to the different chemical environments due to the long-range polarization effect induced by the NaCl/Cu interface and/or the elimination of intermolecular interaction present in the bulk crystal.

Finally, we discuss the differences of the insulating films of MgO and NaCl; the former has been extensively employed in ESR-STM experiments,^{18,24,39,29,40,41} whereas the latter is used in optical-STM experiments for single molecules^{42,43} and deliberately adopted in this study. The role of both insulating films is to decouple electrically the adsorbate from metal substrate, such as single atom or molecule, and access the intrinsic single-adsorbate properties. However, the recent report of the ESR-STM measurements on a molecule by using the MgO film indicated remarkable coupling between the molecule and the metal substrate through the MgO insulating film. Specifically, the ESR signals of $S = 1/2$ were observed on the single iron phthalocyaninato (FePc) molecule^{27,41} even though FePc possesses the intrinsic spin $S = 1$ in the bulk phase and on several surfaces^{44,45}. The authors attributed the change of spin configuration to charge transfers from the metal substrate to the FePc, and the molecular spin became $S = 1/2$. This charge transfer through the MgO film was also reported for other molecules²⁸. In contrast, our result shows that by using the NaCl film, the intrinsic π -radical $S = 1/2$ electron in the TbPc₂ molecule subsisted without charge transfer.

The different behavior observed based on the use of the two insulating materials can be explained by the results of the DFT calculation⁴⁶ which compared the binding energies (E_b) of the NaCl and MgO thin films. The results revealed that E_b was approximately two times higher on MgO than the NaCl surface. The intrinsic difference between the two insulating films can be traced back to the Madelung potential⁴⁶. The MgO film, which consists of divalent ion crystals, yields a much higher value than monovalent NaCl. Thus, the NaCl film employed in our experiment acted as a

“soft” insulating film between the molecule and the metal substrate and thus successfully suppressed the charge transfer and hybridization between them.

In conclusion, we demonstrated ESR-STM measurements on the single TbPc₂ molecule without influences from the metal substrate; this was achieved by utilizing the 2ML NaCl film. We resolved intrinsic π -radical $S = 1/2$ electron delocalization at the Pc ligands that possessed a g -factor equal to 1.84 ± 0.12 . The intercept observed in the plot of the B field versus resonance frequency showed a large deviation from that for the TbPc₂ bulk crystal. The discrepancy can be explained by the intramolecular exchange interaction susceptible to the chemical environment, which is different in bulk crystalline molecules and surface-adsorbed single molecule.

Our ESR-STM measurements in conjunction with the decoupling method can be applied to detect⁴⁷ and manipulate the hyperfine-coupled Tb spins in the TbPc₂ molecule with the minimization of decoherence owing to the coupling to the metal substrate. This can be extended to a study on the magnetic inter- and intramolecular interaction mediated by the π -radical electron in the 1D¹²⁻¹⁵ or 2D¹⁶ network, wherein the localized Tb spins can be potentially used as coupled qubits to achieve molecular-based QIP.

Supporting Information. The following files are available free of charge.

S1. Details of experimental setup

S2. Confirmation of spin-polarized tip with dI/dV spectrum

S3. Acquisition and compensation of transfer function

S4. Statistical analysis of the number of isolated TbPc₂ molecules on the surface (PDF)

Corresponding Author

Ryo Kawaguchi – Institute of Multidisciplinary Research for Advanced Materials (IMRAM, Tagen), Tohoku University, 2-1-1, Katahira, Aoba-Ku, Sendai 980-0877, Japan; <https://orcid.org/0000-0002-1211-3550>; Email: ryo.kawaguchi.a1@tohoku.ac.jp

Tadahiro Komeda – Institute of Multidisciplinary Research for Advanced Materials (IMRAM, Tagen), Tohoku University, 2-1-1, Katahira, Aoba-Ku, Sendai 980-0877, Japan; Department of Chemistry, Graduate School of Science, Tohoku University, Aramaki-Aza-Aoba, Aoba-Ku, Sendai 980-8578, Japan; <https://orcid.org/0000-0003-2342-8184>; Email: tadahiro.komeda.a1@tohoku.ac.jp

Author Contributions

R.K. conducted the measurements and data analysis and wrote the manuscript with advice of K.H. and T.K. R.K. developed the ESR-STM system with the help of T.K., K.H. K.K. and M.Y. synthesized the TbPc₂ molecules. All authors discussed the results and contributed to the writing of the manuscript.

Funding Sources

This study was supported in part by the Grant-in-Aid for Scientific Research (S) (No.19H05621) (R.K., K.H., T.K.) and by the National Natural Science Foundation of China (NSFC, 21971124, 22150710513). Special thanks are devoted for the support from the 111 projects (B18030) from China. K.H., T.K., and R.K. thank the TIA Kakehashi program for their support.

Notes

The authors declare no competing financial interests.

R.K. thanks Andreas Heinrich, Soo-Hyon Phark, and Fabio Donati for fruitful discussions.

- (1) Ladd, T. D.; Jelezko, F.; Laflamme, R.; Nakamura, Y.; Monroe, C.; O'Brien, J. L. Quantum Computers. *Nature* **2010**, *464* (7285), 45-53.
- (2) Awschalom, D. D.; Bassett, L. C.; Dzurak, A. S.; Hu, E. L.; Petta, J. R. Quantum Spintronics: Engineering and Manipulating Atom-Like Spins in Semiconductors. *Science* **2013**, *339* (6124) 1174-1179.
- (3) Kane, B. E. A silicon-based nuclear spin quantum computer. *Nature* **1998**, *393* (6681), 133.
- (4) Loss, D.; DiVincenzo, D. P. Quantum Computation with Quantum Dots. *Phys. Rev. A* **1998**, *57* (1), 120.
- (5) Nowack, K. C.; Koppens, F. H. L.; Nazarov, Y. V.; Vandersypen, L. M. K. Coherent Control of a Single Electron Spin with Electric Fields. *Science* **2007**, *318* (5855), 1430-1433.
- (6) Pla, J. J.; Tan, K. Y.; Dehollain, J. P.; Lim, W. H.; Morton, J. J. L.; Jamieson, D. N.; Dzurak, A. S.; Morello, A. A Single-Atom Electron Spin Qubit in Silicon. *Nature* **2012**, *489* (7417), 541-5.
- (7) Pineda, E. M.; Komeda, T.; Katoh, K.; Yamashita, M.; Ruben, M. Surface Confinement of TbPc₂-SMMs: Structural, Electronic and Magnetic Properties. *Dalton Trans.* **2016**, *45* (46), 18417-18433.

(8) Thiele, S.; Balestro, F.; Ballou, R.; Klyatskaya, S.; Ruben, M.; Wernsdorfer, W. Electrically Driven Nuclear Spin Resonance in Single-Molecule Magnets. *Science* **2014**, *344* (6188), 1135-1138.

(9) Godfrin, C.; Ferhat, A.; Ballou, R.; Klyatskaya, S.; Ruben, M.; Wernsdorfer, W.; Balestro, F. Operating Quantum States in Single Magnetic Molecules: Implementation of Grover's Quantum Algorithm. *Phys. Rev. Lett.* **2017**, *119* (18), 187702.

(10) Godfrin, C.; Thiele, S.; Ferhat, A.; Klyatskaya, S.; Ruben, M.; Wernsdorfer, W.; Balestro, F. Electrical Read-Out of a Single Spin Using an Exchange-Coupled Quantum Dot. *ACS Nano* **2017**, *11* (4), 3984-3989.

(11) Paschke, F.; Birk, T.; Avdoshenko, S. M.; Liu, F.; Popov, A. A.; Fonin, M. Imaging the Single-Electron Ln–Ln Bonding Orbital in a Dimetallofullerene Molecular Magnet. *Small* **2022**, *18* (3), 2105667.

(12) Urdampilleta, M.; Klyatskaya, S.; Cleuziou, J.-P.; Ruben, M.; Wernsdorfer, W. Supramolecular Spin Valves. *Nat. Mater.* **2011**, *10* (7), 502-506.

(13) Urdampilleta, M.; Klayatskaya, S.; Ruben, M.; Wernsdorfer, W. Magnetic Interaction Between a Radical Spin and a Single-Molecule Magnet in a Molecular Spin-Valve. *ACS Nano* **2015**, *9* (4), 4458–4464.

(14) Jenkins, M. D.; Zueco, D.; Roubeau, O.; Aromí, G.; Majer, J.; Luis, F. A Scalable Architecture for Quantum Computation with Molecular Nanomagnets. *Dalton Trans.* **2016**, *45* (42), 16682–16693.

(15) Najafi, K.; Wysocki, A. L.; Park, K.; Economou, S. E.; Barnes, E. Toward Long-Range Entanglement between Electrically Driven Single-Molecule Magnets. *J. Phys. Chem. Lett.* **2019**, *10* (23), 7347–7355.

(16) Amokrane, A.; Klyatskaya, S.; Boero, M.; Ruben, M.; Bucher, J.-P. Role of π -Radicals in the Spin Connectivity of Clusters and Networks of Tb Double-Decker Single Molecule Magnets. *ACS Nano* **2017**, *11* (11), 10750–10760.

(17) Komeda, T.; Isshiki, H.; Liu, J.; Zhang, Y.-F.; Lorente, N.; Katoh, K.; Breedlove, B. K.; Yamashita, M. Observation and Electric Current Control of a Local Spin in a Single-Molecule Magnet. *Nat. Commun.* **2011**, *2* (1), 217.

(18) Baumann, S.; Paul, W.; Choi, T.; Lutz, C. P.; Ardavan, A.; Heinrich, A. J. Electron Paramagnetic Resonance of Individual Atoms on a Surface. *Science* **2015**, *350* (6259), 417–420.

(19) Yang, K.; Paul, W.; Phark, S.-H.; Willke, P.; Bae, Y.; Choi, T.; Esat, T.; Ardavan, A.; Heinrich, A. J.; Lutz, C. P. Coherent Spin Manipulation of Individual Atoms on a Surface. *Science* **2019**, *366* (6464), 509–512.

(20) Wolf, E. L.; Losee, D. L. G-Shifts in the “s-d” Exchange Theory of Zero-Bias Tunneling Anomalies. *Phys. Lett. A* **1969**, *29* (6), 334–335.

(21) Ara, F.; Qi, Z. K.; Hou, J.; Komeda, T.; Katoh, K.; Yamashita, M. A Scanning Tunneling Microscopy Study of the Electronic and Spin States of Bis(Phthalocyaninato)Terbium(III) (TbPc_2) Molecules on Ag(111). *Dalton Trans.* **2016**, *45* (42), 16644–16652.

(22) Zhang, X.; Wolf, C.; Wang, Y.; Aubin, H.; Bilgeri, T.; Willke, P.; Heinrich, A. J.; Choi, T. Electron Spin Resonance of Single Iron Phthalocyanine Molecules and Role of Their Non-Localized Spins in Magnetic Interactions. *Nat. Chem.* **2022**, *14* (1), 59–65.

(23) Schwöbel, J.; Fu, Y.; Brede, J.; Dilullo, A.; Hoffmann, G.; Klyatskaya, S.; Ruben, M.; Wiesendanger, R. Real-Space Observation of Spin-Split Molecular Orbitals of Adsorbed Single-Molecule Magnets. *Nat. Commun.* **2012**, *3* (1), 953.

(24) Bae, Y.; Yang, K.; Willke, P.; Choi, T.; Heinrich, A. J.; Lutz, C. P. Enhanced Quantum Coherence in Exchange Coupled Spins via Singlet-Triplet Transitions. *Sci. Adv.* **2018**, *4* (11), eaau4159.

(25) Yang, K.; Bae, Y.; Paul, W.; Natterer, F. D.; Willke, P.; Lado, J. L.; Ferrón, A.; Choi, T.; Fernández-Rossier, J.; Heinrich, A. J.; Lutz, C. P. Engineering the Eigenstates of Coupled Spin- $\frac{1}{2}$ Atoms on a Surface. *Phys. Rev. Lett.* **2017**, *119* (22), 227206.

(26) Seifert, T. S.; Kovarik, S.; Nistor, C.; Persichetti, L.; Stepanow, S.; Gambardella, P. Single-Atom Electron Paramagnetic Resonance in a Scanning Tunneling Microscope Driven by a Radio-Frequency Antenna at 4 K. *Phys. Rev. Res.* **2020**, *2* (1), 013032.

(27) Willke, P.; Bilgeri, T.; Zhang, X.; Wang, Y.; Wolf, C.; Aubin, H.; Heinrich, A.; Choi, T. Coherent Spin Control of Single Molecules on a Surface. *ACS Nano* **2021**, *15* (11), 17959–17965.

(28) Hollerer, M.; Lüftner, D.; Hurdax, P.; Ules, T.; Soubatch, S.; Tautz, F. S.; Koller, G.; Puschnig, P.; Sterrer, M.; Ramsey, M. G. Charge Transfer and Orbital Level Alignment at Inorganic/Organic Interfaces: The Role of Dielectric Interlayers. *ACS Nano* **2017**, *11* (6), 6252–6260.

(29) Willke, P.; Paul, W.; Natterer, F. D.; Yang, K.; Bae, Y.; Choi, T.; Fernández-Rossier, J.; Heinrich, A. J.; Lutz, C. P. Probing Quantum Coherence in Single-Atom Electron Spin Resonance. *Sci. Adv.* **2018**, *4* (2), eaaq1543.

(30) van Weerdenburg, W. M. J.; Steinbrecher, M.; van Mullekom, N. P. E.; Gerritsen, J. W.; von Allwörden, H.; Natterer, F. D.; Khajetoorians, A. A. A Scanning Tunneling Microscope Capable of Electron Spin Resonance and Pump–Probe Spectroscopy at MK Temperature and in Vector Magnetic Field. *Rev. Sci. Instrum.* **2021**, *92* (3), 033906.

(31) Repp, J.; Meyer, G.; Stojković, S. M.; Gourdon, A.; Joachim, C. Molecules on Insulating Films: Scanning-Tunneling Microscopy Imaging of Individual Molecular Orbitals. *Phys. Rev. Lett.* **2005**, *94* (2), 026803.

(32) Jaculbia, R. B.; Imada, H.; Miwa, K.; Iwasa, T.; Takenaka, M.; Yang, B.; Kazuma, E.; Hayazawa, N.; Taketsugu, T.; Kim, Y. Single-Molecule Resonance Raman Effect in a Plasmonic Nanocavity. *Nat. Nanotechnol.* **2020**, *15* (2), 105–110.

(33) Zhang, Y.; Meng, Q.-S.; Zhang, L.; Luo, Y.; Yu, Y.-J.; Yang, B.; Zhang, Y.; Esteban, R.; Aizpurua, J.; Luo, Y.; Yang, J.-L.; Dong, Z.-C.; Hou, J. G. Sub-Nanometre Control of the Coherent Interaction between a Single Molecule and a Plasmonic Nanocavity. *Nat. Commun.* **2017**, *8* (1), 15225.

(34) Barhoumi, R.; Amokrane, A.; Klyatskaya, S.; Boero, M.; Ruben, M.; Bucher, J.-P. Screening the 4f-Electron Spin of TbPc_2 Single-Molecule Magnets on Metal Substrates by Ligand Channeling. *Nanoscale* **2019**, *11* (44), 21167–21179.

(35) Komijani, D.; Ghirri, A.; Bonizzoni, C.; Klyatskaya, S.; Moreno-Pineda, E.; Ruben, M.; Soncini, A.; Affronte, M.; Hill, S. Radical-Lanthanide Ferromagnetic Interaction in a Tb^{III} Bis-Phthalocyaninato Complex. *Phys. Rev. Mater.* **2018**, *2* (2), 024405.

(36) Freysoldt, C.; Rinke, P.; Scheffler, M. Controlling Polarization at Insulating Surfaces: Quasiparticle Calculations for Molecules Adsorbed on Insulator Films. *Phys. Rev. Lett.* **2009**, *103* (5), 056803.

(37) Repp, J.; Meyer, G. Scanning Tunneling Microscopy of Adsorbates on Insulating Films. From the Imaging of Individual Molecular Orbitals to the Manipulation of the Charge State. *Appl. Phys. A* **2006**, *85* (4), 399–406.

(38) Boukhvalov, D. W.; Dobrovitski, V. V.; Kögerler, P.; Al-Safer, M.; Katsnelson, M. I.; Lichtenstein, A. I.; Harmon, B. N. Effect of Ligand Substitution on the Exchange Interactions in {Mn₁₂}-Type Single-Molecule Magnets. *Inorg. Chem.* **2010**, *49* (23), 10902–10906.

(39) Singha, A.; Willke, P.; Bilgeri, T.; Zhang, X.; Brune, H.; Donati, F.; Heinrich, A. J.; Choi, T. Engineering Atomic-Scale Magnetic Fields by Dysprosium Single Atom Magnets. *Nat. Commun.* **2021**, *12* (1), 4179.

(40) Willke, P.; Singha, A.; Zhang, X.; Esat, T.; Lutz, C. P.; Heinrich, A. J.; Choi, T. Tuning Single-Atom Electron Spin Resonance in a Vector Magnetic Field. *Nano Lett.* **2019**, *19* (11), 8201–8206.

(41) Zhang, X.; Wolf, C.; Wang, Y.; Aubin, H.; Bilgeri, T.; Willke, P.; Heinrich, A.; Choi, T. Electron Spin Resonance of Single Iron Phthalocyanine Molecules and Role of Their Non-Localized Spins in Magnetic Interactions. *Nat. Chem.* **2022**, *14* (1), 59–65.

(42) Jaculbia, R. B.; Imada, H.; Miwa, K.; Iwasa, T.; Takenaka, M.; Yang, B.; Kazuma, E.; Hayazawa, N.; Taketsugu, T.; Kim, Y. Single-Molecule Resonance Raman Effect in a Plasmonic Nanocavity. *Nat. Nanotechnol.* **2020**, *15* (2), 105–110.

(43) Imada, H.; Imai-Imada, M.; Miwa, K.; Yamane, H.; Iwasa, T.; Tanaka, Y.; Toriumi, N.; Kimura, K.; Yokoshi, N.; Muranaka, A.; Uchiyama, M.; Taketsugu, T.; Kato, Y. K.; Ishihara, H.; Kim, Y. Single-molecule laser nanospectroscopy with micro–electron volt energy resolution. *Science* **2021**, *373* (6550) 95-98.

(44) Tsukahara, N.; Noto, K.; Ohara, M.; Shiraki, S.; Takagi, N.; Takata, Y.; Miyawaki, J.; Taguchi, M.; Chainani, A.; Shin, S.; Kawai, M. Adsorption-Induced Switching of Magnetic Anisotropy in a Single Iron(II) Phthalocyanine Molecule on an Oxidized Cu(110) Surface. *Phys. Rev. Lett.* **2009**, *102* (16), 167203.

(45) Hiraoka, R.; Minamitani, E.; Arafune, R.; Tsukahara, N.; Watanabe, S.; Kawai, M.; Takagi, N. Single-molecule quantum dot as a Kondo simulator. *Nature Communications* **2017**, *8* (16012).

(46) Tiffany Chen, H.-Y.; Pacchioni, G. Properties of Two-Dimensional Insulators: A DFT Study of Co Adsorption on NaCl and MgO Ultrathin Films. *Phys. Chem. Chem. Phys.* **2014**, *16* (39), 21838–21845.

(47) Müllegger, S.; Tebi, S.; Das, A. K.; Schöfberger, W.; Faschinger, F.; Koch, R. Radio Frequency Scanning Tunneling Spectroscopy for Single-Molecule Spin Resonance. *Phys. Rev. Lett.* **2014**, *113* (13), 133001.

Supporting Information

Spatially Resolving Electron Spin Resonance of π -Radical in Single-molecule Magnet

Ryo Kawaguchi^a, Katsushi Hashimoto^{b,c}, Toshiyuki Kakudate^d, Keiichi Katoh^e, Masahiro Yamashita^{f,g}, and Tadahiro Komeda^{a,c}.

^a Institute of Multidisciplinary Research for Advanced Materials (IMRAM, Tagen), Tohoku University, Sendai 980-0877, Japan

^b Department of Physics, Graduate School of Sciences, Tohoku University, Sendai 980-8578, Japan

^c Center for Science and Innovation in Spintronics (Core Research Cluster), Tohoku University, Sendai 980-8577, Japan

^d Department of Industrial Systems Engineering National Institute of Technology (KOSEN), Hachinohe College, 16-1 Uwanotai, Tamonoki, Hachinohe, 039-1192, Japan

^e Department of Chemistry, Graduate School of Science, Josai University, Sakado, Saitama 350-0295, Japan

^f Department of Chemistry, Graduate School of Science, Tohoku University, Sendai 980-8578, Japan

^g School of Materials Science and Engineering, Nankai University, Tianjin 300350, China

S1. Details of experimental setup

S2. Confirmation of spin-polarized tip with dI/dV spectrum

S3. Acquisition and compensation of transfer function

S4. Statistical analysis of the number of isolated TbPc₂ molecules on the surface

S1. Details of the experimental setup

All experiments were performed in an ultrahigh-vacuum condition and at the sample temperature of 0.4 K achieved by the ^3He cooling system (Unisoku USM1300). The cooling system was also equipped with a superconductor magnet (Cryogenic Ltd.) which was able to generate the out-of-plane magnetic field up to 11 T. We introduced the RF signal through the high-frequency cables connected to the tip bias line (Figure S1). The SMP-type feedthrough (Solid Sealing Technology, FA33179-1FF) create the connection between the ambient and the internal vacuum chamber (IVC), which had a lower insertion-loss performance than that of the standard SMA-type. We employed the semi-rigid cable of SC-219/50-SCN-CN (COAX Co., Ltd.) from this connector to the 1 K pot (orange line), and from the 1 K pot to the ultrahigh vacuum (UHV) feedthrough (green line), SC-119/50-SCN-CN (COAX CO., LTD). In the UHV chamber, the connection to the STM tip (blue line) was established by using the flexible coaxial cable (Cooner Wire, CW2040-3650F). For the line of the tunneling current, we used a SMA-type connector (COSMOTEC Co., C34SMR1) and flexible coaxial cable (same as that used for the RF line, as shown by the blue line in Figure S1). The continuous sinusoidal signal from the RF generator (Keysight, N5193A) was applied to the tunneling junction (V_{RF}) through the bias Tee (SigaTek, SB15D2) and combined with the DC bias voltage (V_{DC}). The cable shown with the yellow line in the figure is flexible coaxial cable (Mini-Circuits, TMP40-6FT-KMKG+).

For the lock-in detection, we modulated the amplitude of the RF signal (hence the RF bias voltage (V_{RF})) in a chopping scheme at a frequency of $f_{\text{mod}} = 431$ Hz. The resulting V_{RF} -induced tunnel current was detected with a lock-in amplifier (NF, LI5650) after an amplification by using the current amplifier (Femto, DLPCA-200) with the bandwidth which covered the f_{mod} . The lock-in output ($V_{\text{lock-in}}$) corresponded to the root-mean-square value of the V_{RF} -induced tunnel current;

it is defined as the V_{RF} -induced variation in the tunnel current (ΔI). The ESR signal was acquired with a relatively weak feedback loop with the spin-polarized tip prepared by picking up a few Fe atoms from the Cu surface, while STM images were obtained at the constant-current mode.

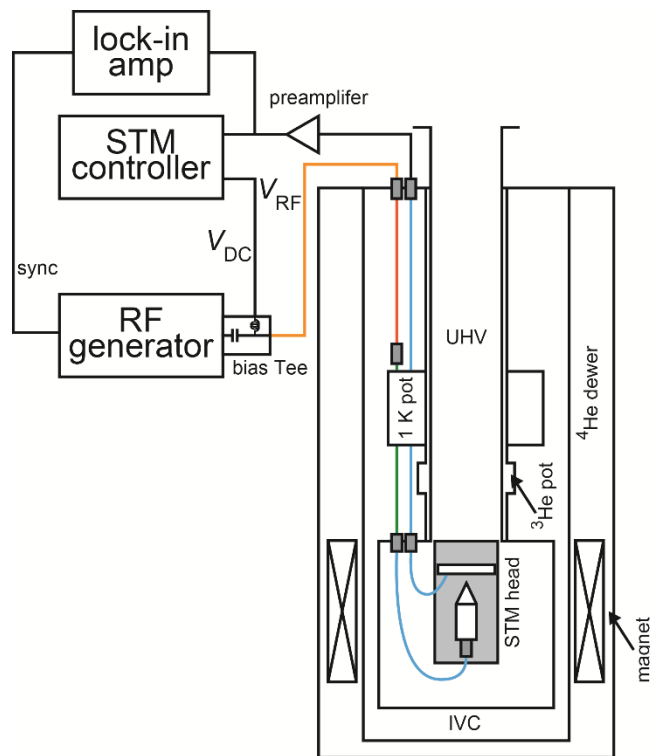


Figure S1. Schematic of radiofrequency (RF) cabling in the cryostat and outside of the measurement setup area used for electron spin resonance measurements.

S2. Spin-polarized tip with dI/dV spectra

Figure S2(a) shows the dI/dV spectrum acquired with a nonmagnetic PtIr tip at the lobe position of the TbPc₂ molecule absorbed on the Cu(100) surface in the absence of the magnetic field. The sharp peak near the Fermi level corresponds to the Kondo peak. In the magnetic field ($B_{\text{ext}} = 500$ mT), as shown by the black curve in Figure S2(b), this peak splits into two peaks marked by arrows, thus resulting in the symmetric spectrum concerning the bias polarity. The obtained splitting was caused by spin excitation inelastic tunneling spectroscopy (IETS) owing to the transition between the Zeeman split state $m = \pm 1/2$ of the π -radical electron of $S = 1/2$. Conversely, the dI/dV spectrum obtained with the spin-polarized tip, which was prepared by picking up a few Fe atoms from the Cu surface (red curve in Figure S2b), shows the asymmetric shape owing to the selection rule for spin excitation with tunneling electron^{1,2}. By using this method, we confirmed the tip polarization before we conducted the ESR measurements.

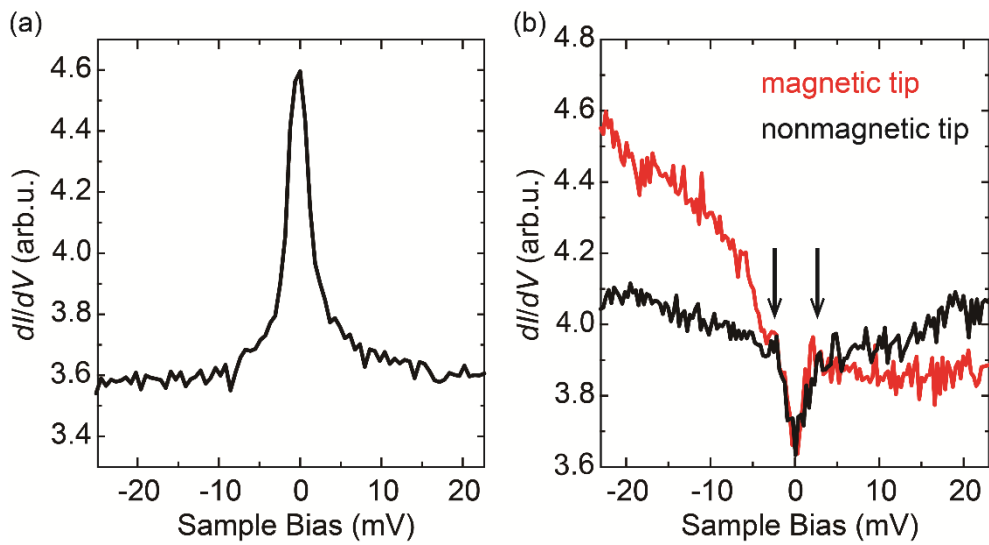


Figure S2. Preparation of spin-polarized scanning tunneling microscopy (STM) tip. (a) dI/dV spectrum acquired at the lobe position of TbPc_2 molecule absorbed on the $\text{Cu}(100)$ surface in the absence of a magnetic field. (b) dI/dV spectra acquired with (red curve) and without (black curve) a magnetic tip in the presence of a magnetic field ($B_{\text{ext}} = 500$ mT). All dI/dV spectra were acquired at the same conditions ($V_{\text{DC}} = 25$ mV, $I = 500$ pA, $V_{\text{mod}} = 1$ mV, $f_{\text{mod}} = 431$ Hz).

S3. Acquisition and compensation of transmission

The transmission of the entire RF signal line (Figure S1) has a specific frequency dependency owing to the characteristics of the RF components (such as cables, connectors, and feedthrough). As this frequency-dependent transmission makes the identification of the ESR peaks difficult, it is required to calibrate the transmission characteristics prior to ESR measurements. In frequency sweeping ESR-STM measurements with the constant RF source power (P_{RF}), frequency-dependent transmissions modify the amplitude of the RF voltage (V_{RF}) applied to the tunneling junction, and hence alter the ESR signal obtained as the tunnel current enhancement (ΔI), thus leading to the artifact in the ESR spectrum. This artifact can be misinterpreted as an ESR signal, thus making it difficult to identify the actual ESR signal.

To compensate for the frequency-dependent influence of the transmission, we tuned P_{RF} by the following procedure, as reported previously³. First, we quantified the V_{RF} amplitude by rectifying the nonlinearity in the I – V characteristic obtained from the Ag(111) surface state⁴. The Ag(111) surface was prepared with repeated Ar^+ ion sputtering and annealing at 773 K. As shown in the STM images (Figure S3(a)), the prepared surface shows the monolayer steps with hexagonal atomic structures (inset), which constitute evidence that an atomically clean surface was prepared. The dI/dV spectrum obtained on the Ag(111) surface (blue spectrum in Figure S3(b)) shows the step-like structure and indicates the onset of the surface state. The application of the continuous wave RF signal ($P_{RF} = -5 \text{ dBm}$, $f = 19 \text{ GHz}$) broadens the step structure (black spectrum in Figure S3(b)). We fitted both spectra with an arcsine function and determined the V_{RF} amplitude to be 25 mV at the specific RF condition. To evaluate the V_{RF} variation as a function of P_{RF} , we first measured the ΔI based on the $V_{\text{lock-in}}$, as described in S1, while we swept P_{RF} at a constant RF frequency ($f = 19 \text{ GHz}$). The $V_{\text{lock-in}}$ was then scaled to V_{RF} by using

the relation between V_{RF} and $V_{lock-in}$ obtained by the surface-state measurement described above. By using this method, we determined the P_{RF} which corresponded to any required V_{RF} ³.

Next, we acquired the RF transmission on the Ag(111) surface by sweeping the frequency in the range of 18–25 GHz at a constant power setting equal to $P_{RF} = +5$ dBm. The tunneling condition of V_{DC} was adjusted to the Ag(111) surface state onset of -70 mV (see Figure S3(b)) during the application of an RF signal for rectification of nonlinearity of the I – V curve. Herein, we set the tunneling current to 500 pA, which was higher than that used in our ESR measurement (10 pA). The higher tunneling current increased the V_{RF} and thus allowed us to obtain a more accurate relative intensity of the RF signal over the entire frequency range, especially in the frequency region in which the signal was strongly attenuated within the RF line. The RF transmission can be determined by dividing $V_{lock-in}$ by the source power of P_{RF} . Figure S3(c) shows the RF transmission measured on an Ag(111) surface in the frequency range of 18–25 GHz at a constant $P_{RF} = +5$ dBm.

Finally, to compensate for the RF transmission, we tuned P_{RF} (as plotted in Figure S3(d)) which was calculated from the obtained transmission function based on a method described previously³. The result (Figure S3(e)) obtained on the NaCl/Cu(100) surface demonstrates that we can produce a constant $V_{RF} = 5$ mV over the frequency range of 18–25 GHz used in our ESR-STM measurements.

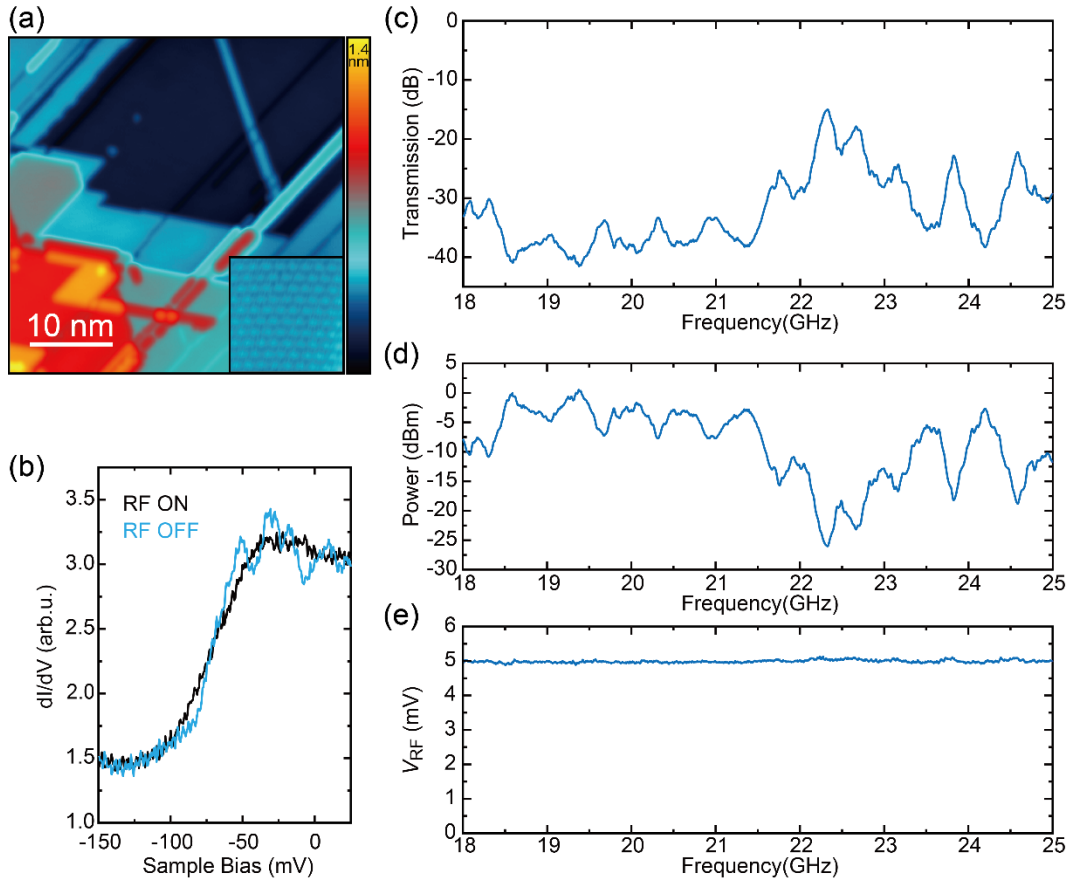


Figure S3. Compensation of RF transmission at the tunneling junction. (a) Typical large-scale STM image of Ag(111) surface (scanning condition: $V_{DC} = 0.9$ V and $I = 18$ pA). The inset shows an image at an atomic resolution (scanning condition: $V_{DC} = 70$ mV and $I = 500$ pA). (b) dI/dV spectra of step-like Ag(111) surface state with (black curve) and without (blue curve) RF signal ($P_{RF} = -5$ dBm, $f = 19$ GHz). The applied continuous RF signal broadened the step-like surface state of Ag(111) owing to the application of the V_{RF} at the tunnel junction; the V_{RF} amplitude was estimated to be 25 mV. (c) RF transmission of frequency range 18–25 GHz at a constant RF source power equal to $P_{RF} = 5$ dBm. (d) The RF source power used to compensate the frequency-dependent RF transmission and create constant V_{RF} at tunnel junction. (e) The constant V_{RF} amplitude of 5 mV was achieved by utilizing a compensated source power.

S4. Statistical analysis of the number of isolated TbPc2 molecules on the surface

As shown in Figure 1(b) in the main text, there are several isolated single TbPc₂ molecules over the Cu(100) surface, while a few isolated single molecules exist on the NaCl surface where most molecules either aggregate at the edge of the NaCl island or make clusters. The same tendency was observed in other areas of the same sample as shown in Figure S4. We estimated the densities of the isolated molecule on the Cu and NaCl surfaces to be 17 molecules per 1618 nm^2 $\sim 1.1 \times 10^{-3} \text{ nm}^{-2}$, and 2 molecules per $482 \text{ nm}^2 \sim 4.1 \times 10^{-3} \text{ nm}^{-2}$, respectively. We performed the same analysis in ten different areas, including those shown in Figures 1b and S4. The averaged density ratio of the isolated molecules found on the Cu and NaCl surfaces was equal to 3:1.

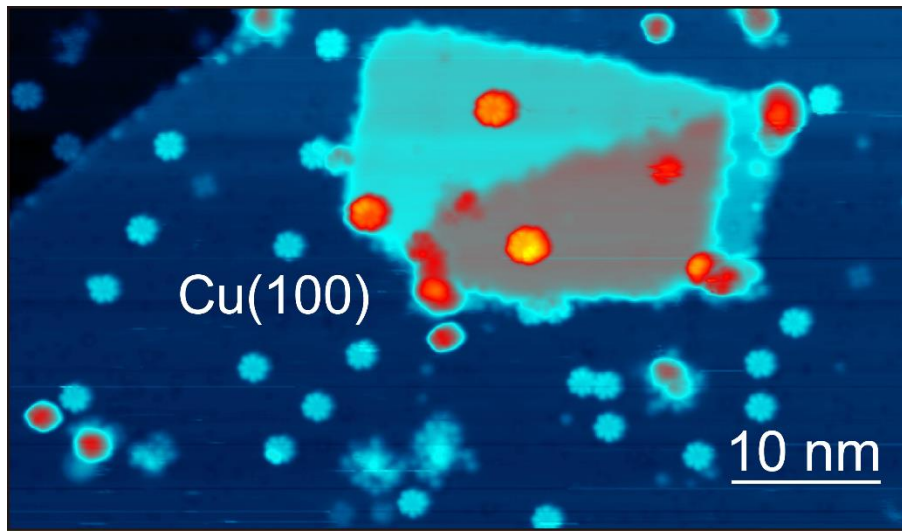


Figure S4. STM image of TbPc₂ molecules adsorbed on bare Cu(100) and 2 ML NaCl/Cu(100) surfaces. Scanning conditions: $V_{\text{DC}} = 1.4 \text{ V}$ and $I = 10 \text{ pA}$.

- (1) Loth, S.; von Bergmann, K.; Ternes, M.; Otte, A. F.; Lutz, C. P.; Heinrich, A. J. Controlling the State of Quantum Spins with Electric Currents. *Nat. Phys.* **2010**, *6* (5), 340–344.
- (2) von Bergmann, K.; Ternes, M.; Loth, S.; Lutz, C. P.; Heinrich, A. J. Spin Polarization of the Split Kondo State. *Phys. Rev. Lett.* **2015**, *114* (7), 076601.
- (3) Paul, W.; Baumann, S.; Lutz, C. P.; Heinrich, A. J. Generation of Constant-Amplitude Radio-Frequency Sweeps at a Tunnel Junction for Spin Resonance STM. *Rev. Sci. Instrum.* **2016**, *87* (7), 074703.
- (4) van Weerdenburg, W. M. J.; Steinbrecher, M.; van Mullekom, N. P. E.; Gerritsen, J. W.; von Allwörden, H.; Natterer, F. D.; Khajetoorians, A. A. A Scanning Tunneling Microscope Capable of Electron Spin Resonance and Pump–Probe Spectroscopy at MK Temperature and in Vector Magnetic Field. *Rev. Sci. Instrum.* **2021**, *92* (3), 033906.